A PON Monitoring System Integrating Fault Detection and Localization

Xuan Zhang, Tianfeng Yang, and Xinhong Jia

***Abstract*—We propose and experimentally demonstrate an integrated passive optical network monitoring system for fault detection and localization. Fault detection technology is based on the recognition of reflection spectrum generated by each single fiber Bragg grating, which can support large-capacity user fiber fault monitoring. Fault localization method uses two different total received powers measured by an optical power meter to solve the established equation, and it shows a good accuracy compared with the OTDR measurement results. Fault detection and localization are carried out separately but share the same transmitter module. The introduction of the additional module ensures that the troubleshooting does not affect other normal user data communication. We also investigate the dynamic range requirements of the fault detection technology and the measurement error of the fault localization method. The calculation results show the required dynamic range for the recognition device can be maintained within a small range and the use of high-accuracy optical power meter can reduce the measurement error. The proposed monitoring system can simultaneously provide a large-capacity fault detection technology and high-accuracy fault localization method in a cost-sensitive passive optical network market.**

***Index Terms*—Fault detection, fault localization, network monitoring system, passive optical network (PON).**

I. Introduction

THE surging demand for consumer-driven high bandwidth applications for the residential market, such as high-definition television (HDTV), Internet protocol television (IPTV), interactive gaming, online shopping or streaming etc., has led to a large-scale global investment and deployment of passive optical network (PON)-based access technology. Over last two decades, PON has received a considerable amount of attraction for their efficiency and cost-effectiveness in comparison to the older traditional copper-based networks [1], [2], [3]. PON architectures have increasingly become the preferred choice among many global markets, allowing service providers to meet performance demands effectively and efficiently in access networks [4], [5], [6]. Up to date, more than 20 operators in the world have deployed XG-PON networks, more than 30 operators have released XG-PON services, and more than 100 operators have released Gigabit services. At the same time, broadband operators around the world are shifting gear and deploying next-generation PON (NG-PON) in their fiber networks [7], [8]. For instance, NG-PON2 has been successfully deployed in live networks at some of the biggest service providers such as Verizon in the USA, CityFiber GB, Northpower Fiber NZ, Pilot Mannhatan NY/USA. The increasing success of the PON deployment worldwide makes its scale continue to grow, however, the maintenance and management of a PON is increasingly prominent. Some service providers have reported that more than 80% of installed PON failures occurs within the distribution/drop segments of the network [9]. In addition, the physical infrastructure is usually not entirely visible to the network management system (NMS) in the current PON systems. Consequently, traditional inefficient troubleshooting methods increase the operational cost and customer dissatisfaction. To ensure the quality and reliability of PON access network services, especially the fiber optics-based infrastructure for high-speed data and information distribution, an effective optical layer monitoring system is essential [10].

The optical time domain reflectometer (OTDR) is an effective tool to characterize an optical link in point-to-point (P2P) network architecture. Events such as splices, connectors, bends, breaks, or flaws in the fiber can be identified by OTDR. However, OTDR is not effective for point-to-multipoint (P2MP) networks like PONs since the backscattered and reflected powers from all network branches converge into an aggregated trace at the central office (CO) [11], [12]. That is, OTDR cannot identify the specific fault branch in several branches, especially when the distance difference between the branches is small. Therefore, many PON monitoring schemes have been widely proposed in recent years [9], [12], [13], [14], [15], [16], [17]. These existing schemes are designed to identify which branch in the network is faulty, i.e., fault detection. The first and second objective of any PON monitoring system are fault detection and fault localization, respectively [9]. Fault localization is to find the exact location of a fault within the faulty branch. Unfortunately, few reported schemes can achieve both objective at the same time. For most of existing schemes, it is generally necessary to use OTDR to locate the fault after the fault detection is completed. Obviously, the use of OTDR is not only detrimental to the integration of the entire monitoring system, but also violates the PON market's pursuit of cost-effectiveness.

Manuscript received 18 May 2022; revised 5 August 2022; accepted 24 August 2022. Date of publication 29 August 2022; date of current version 6 September 2022. This work was supported by the National Natural Science Foundation of China under Grant 61901289. *(Corresponding author: Xuan Zhang.)*

Xuan Zhang is with the College of Physics and Electronic Engineering, Sichuan Normal University, Chengdu 610101, China, and also with the College of Electronic Science and Engineering, University of Electronic Science and Technology of China, Chengdu 611731, China (e-mail: xuanzhang@sicnu.edu.cn).

Tianfeng Yang and Xinhong Jia are with the College of Physics and Electronic Engineering, Sichuan Normal University, Chengdu 610101, China (e-mail: 20200991025@stu.sicnu.edu.cn; jiaxh_0@126.com).

Digital Object Identifier 10.1109/JPHOT.2022.3202177

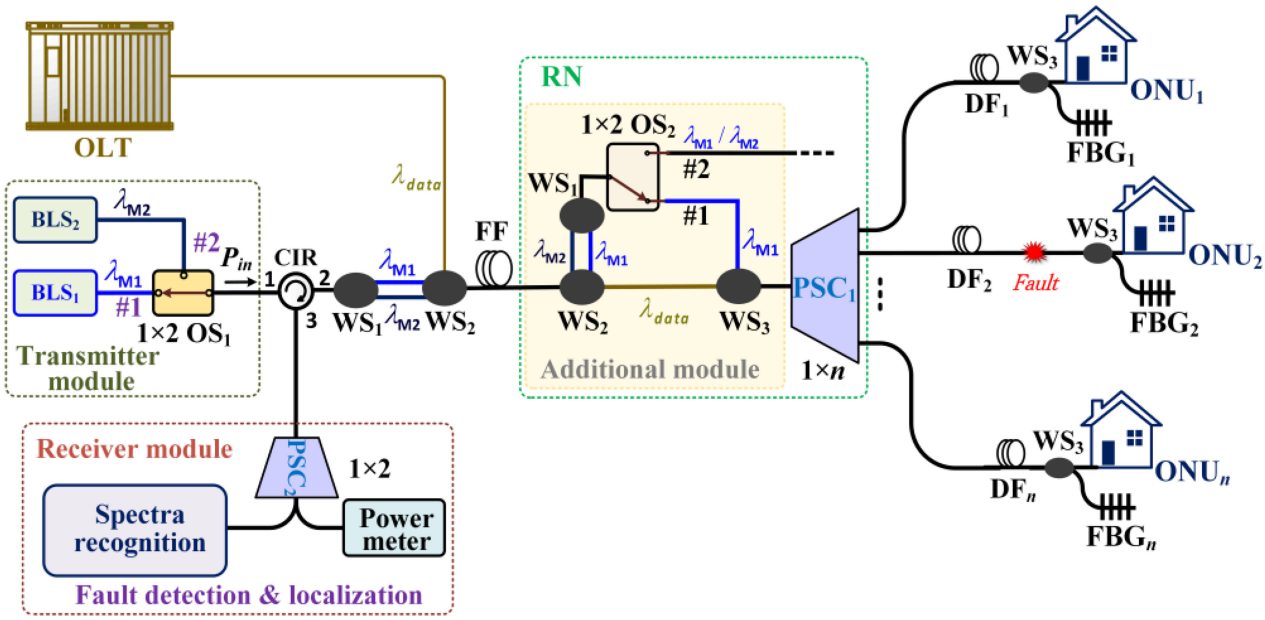

Fig. 1. Schematic diagram of the integrated PON monitoring system.

In this paper, we propose an integrated PON monitoring system that shares the same transmitter module during fault detection and localization. Each drop fiber (DF) (also known branch) link is equipped with a single fiber Bragg grating (FBG) with a different central reflection wavelength (CRW). The objective of fault detection can be simply and effectively achieved after each FBG is interrogated by an unmodulated broadband light source (BLS) signal. With the same transmitter module and an additional optical power meter, the objective of fault localization can be easily achieved using the established equation. The comparison between the results calculated by the established equation and the measurement results of OTDR shows that the fault localization method has good accuracy. A simple additional module is added at the remote node (RN) of the proposed PON monitoring system, which causes no interference with normal data communication during troubleshooting. The simple structure of the proposed PON monitoring system may be welcomed in the cost-sensitive PON market. Compared with [18], the current work is a new and more practical solution, which is mainly manifested in three aspects: i) The current work provides a complete solution for the integration of fault detection and localization, and the compatibility of fault detection technology and fault localization method is also tested in the same PON monitoring system; ii) The use of an unmodulated broadband continue-wave detection source in the current work cannot only make the transmitter module simpler, but also effectively reduce the effect of temperature on the FBG; iii) The detection signal in the current work is easier to generate and the power is more stable, which can make it more practical and widespread in practical engineering. To our best knowledge, the PON monitoring system for fault detection and localization without OTDR assistance have rarely been reported. Furthermore, we also investigate the dynamic range requirements of the fault detection technology and the measurement errors of the fault localization method.

II. Principle and Design

The integrated PON monitoring system is schematically illustrated in Fig. 1. The transmitter module consists of two BLSs and a 1×2 optical switch (OS). For these two BLSs, the center wavelength of one BLS is 1650 nm, and the center wavelength of the other is set to has the same fiber attenuation coefficient as 1650 nm in the fiber under test. The detection signal (i.e., λ_{M1} or λ_{M2}) and the traffic data from the optical line terminal (OLT) are coupled through a wavelength selector (WS) and sent into the feeder fiber (FF). An additional module is added before the $1 \times n$ power splitter/combiner (PSC) at the RN, which consists of a 1×2 OS and three WSs. The wavelength channels corresponding to WS_1, WS_2 and WS_3 are $\{\lambda_{M1}, \lambda_{M2}\}$, $\{\lambda_{M1}, \lambda_{M2}, \lambda_{data}\}$ and $\{\lambda_{M1}, \lambda_{data}\}$, respectively. For the 1×2 OS_2, channel #1 and channel #2 are used for fault detection and fault localization, respectively. By default, the 1×2 OS_2 is placed on channel #1. The detection signal of λ_{M1} and the traffic data would be separated at the WS_2 and combined at the WS_3, and they reach the WS_3 through the channel #1 of the OS_2 and the patch cord between the WS_2 and WS_3, respectively. The use of multiple WSs does introduce extra loss, but does not seriously affect traffic data transmission. Note that WSs used in this system usually has a low insertion loss. Redundancy proposed to be considered in the power budget of a PON system may cover most of the extra power loss caused by the introduction of multiple WSs. At the $1 \times n$ PSC, the detection signal is split into n sub-signal and broadcasted to each DF links. Each FBG with a different CRW is configured at the end of the DF link, which is located physically close to the optical network unit (ONU). The reflected signals generated by each FBG are converged into the FF via the $1 \times n$ PSC, and then returned to the receiver module at the CO through a circulator (CIR).

For the proposed PON monitoring system, fault detection and localization need to be carried out sequentially. Here, we can

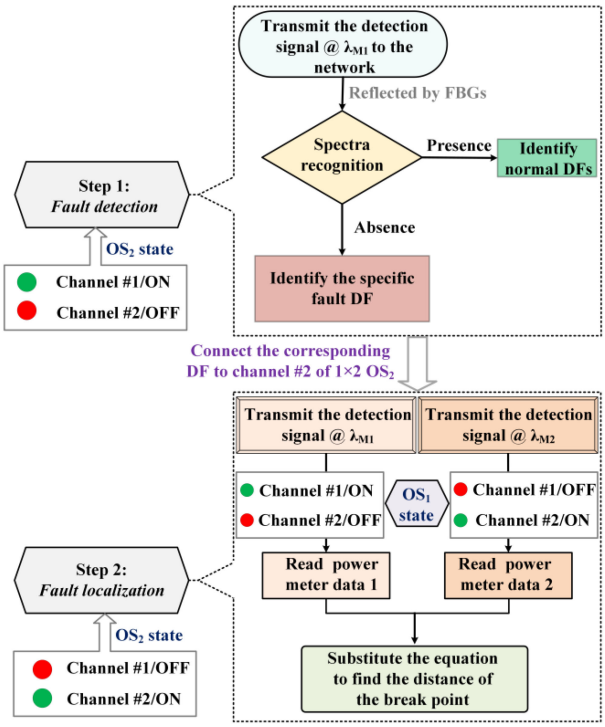

Fig. 2. The workflow of the integrated PON monitoring system.

divide them into two steps, as illustrated in Fig. 2. Since the final recognition is performed in the frequency domain, the fault detection technology proposed here is very suitable for high-density PONs. It is known that the final recognition in the time domain is closely related to the distance difference between each DF link. In the process of fault detection, features of the reflected spectra are used to access the status of the DF links. For instance, a strong reflection peak indicates that the DF link is normal, while a severely attenuated one shows faulty. For the proposed monitoring scheme in Fig. 1, the reflection spectrum for each DF is a function of wavelength, which can be expressed as

$$\begin{aligned} P_i(\lambda)_{(\mathrm{dBm})} = {} & P_0(\lambda) - \alpha_{CIR} - 4\alpha_{WS1} - 4\alpha_{WS2} \\ & - 4\alpha_{WS3} - 2\alpha_l - 2\alpha_{OS2} - 2\alpha_{PSC1} \\ & - 10\log_{10}\left[1 - R_i(\lambda)\right] - \alpha_{PSC2} \end{aligned} \quad (1)$$

where $P_0(\lambda)$ is the part of the power emitted from the transmitter module corresponding to the reflection spectrum of an FBG. α_{CIR}, α_{WS}, α_{OS2}, α_{PSC1} and α_{PSC2} represent the insertion loss of the CIR, WS, OS_2, PSC_1 and PSC_2, respectively. α_l is the fiber attenuation loss, which is composed of the FF and corresponding DF i link ($i = 12, \ldots, n$). $R_i(\lambda)$ is the reflection spectrum function of the FBG used on the DF_i link. Note that the FBGs may be easily broken and influenced by many factors. In practical application, a protection sleeve can be installed on the outside of the FBG to increase its mechanical strength. It is known that changes in temperature may cause a shift in the CRW of the FBG. Note that the application scenario of the proposed system is an access network. That is, all end-users are located in a limited geographic area. The response of each FBG with a different CRW to changes in temperature is roughly the same. In the final spectra recognition, the CRWs of the individual FBG reflection spectra do not overlap because they are shifted by the same magnitude and direction. That is, the effect of temperature on the FBG would not cause the failure of fault detection.

Since the reflection bandwidth of each FBG is much smaller than the spectral width of the BLS, the return signal at the CO would show the complete reflection spectrum of each FBG after being interrogated by the BLS_1. All FBG reflection spectra can be distinguished from each other by different CRWs. Note that the introduction of reflection bandwidth on the CRW can further increase the monitoring capacity of the fault detection technology. The absence of a certain reflection spectrum indicates a failure (e.g., a break) of the corresponding DF link. However, when a failure occurs at any distance on the DF link between the PSC_1 and the ONU, the reflection peak may be absent without difference. That is, like other existing PON monitoring technologies, this fault detection technology can only provide a binary decision on the status (i.e., normal, or faulty) of one and several DF links.

Recall that any PON monitoring system should include both fault detection and localization. Therefore, the complete workflow can be divided into two steps, as shown in Fig. 2. The basic process of step 1 can be simply summarized as: the BLS_1 in the transmitter module transmits the detection signal of λ_{M1} to the PON, and the receiver module assesses the status of each DF link by identifying the absence or presence of the configured FBG reflection spectrum. Note that both OS_1 and OS_2 are placed on channel #1 at this step. The specific details of this step can be found in the above-mentioned schematic description of Fig. 1. After the fault DF link is successfully detected in step 1, the corresponding fault DF link is connected to the channel #2 of OS_2. Next, the process of locating the fault can be performed, as described in step 2 of Fig. 2. In the process of fault localization, the detection signals of λ_{M1} and λ_{M2} successively interrogate the corresponding fault DF, which is realized by 1×2 OS_1 switching from channel #1 to channel #2. The optical power meter in the receiver module would separately record two power values. Finally, the location of the breakpoint can be calculated by substituting the two recorded power values into the established equation. Here, we suppose that the length of the FF is L_{FF} and a break occurs on a DF link (e.g., DF_2). From an OTDR perspective, faults (e.g., breaking, bending, splicing, etc.) on fiber optic links can be broadly classified into reflective and non-reflective events. Recall that the existing fault detection schemes are proposed to solve the problem of OTDR's failure in P2MP networks. It is worth pointing out that some non-reflective events (e.g., macrobends, etc.) may also be identified by these fault detection scheme. However, most of the existing fault detection schemes seem to only involve the event of fiber breakage, especially in the experimental verification. These schemes can guarantee rigor while discarding some types of fault events, since the magnitude of the returned signal alone is not sufficient to distinguish the type of fault event. Like other existing schemes, the fault detection technology in the proposed PON monitoring system is also dedicated to solving the fiber break event. Naturally, the supporting fault localization method only needs to complete the location of the fiber break point. As mentioned earlier, the fault detection is the first objective of

any PON monitoring system. That is, the established equation models used in the fault localization method in the following mainly focus on a reflective event (i.e., fiber break). For this breakpoint, the location on the DF link and the return loss are set to x_b (the starting zero point at the RN) and RL_b, respectively. That is, a return loss RL_b [dB] is introduced into the fiber at the break location x_b. The Rayleigh backscattering occurs when a fraction of scattered light is recaptured and back-reflected towards the launch end within the optical fiber [19]. Obviously, the optical components and fiber links attenuate the input signal while the back-scattered and reflected signal contribute to the final received power. Then, the total backscattered/reflected power (P_{TB}) [mW] of the proposed monitoring system in Fig. 1 can be calculated as

$$\begin{aligned} P_{TB(i)} = P_{in(i)} \Bigg\{ & 10^{\left(-\frac{DIR}{10}\right)} + 10^{\left(-\frac{RL_{WS1}+RL_{WS2}}{10}\right)} \\ & + RAY_i(L_{FF}) \cdot 10^{\left(-\frac{IL_{WS1i}+IL_{WS2i}}{5}\right)} \\ & + T_i^2(L_{FF}) \cdot 10^{\left(-\frac{IL_{WS1i}+IL_{WS2i}}{5}\right)} \\ & \cdot \left[10^{\left(-\frac{RL_{WS1}+RL_{WS2}}{10}\right)} + 10^{\left(-\frac{IL_{WS1i}+IL_{WS2i}}{5}\right)} \right. \\ & \left. \cdot\ 10^{\left(-\frac{RL_{OS2}}{10}\right)} \right] \\ & + [RAY_i(L_{FF}+x_b) - RAY_i(L_{FF})] \\ & \cdot 10^{\left(-\frac{2IL_{WS1i}+2IL_{WS2i}+IL_{OS2i}+\alpha_C}{5}\right)} \\ & + T_i^2(L_{FF}+x_b) \cdot 10^{\left(-\frac{2IL_{WS1i}+2IL_{WS2i}+IL_{OS2i}+\alpha_C}{5}\right)} \\ & \cdot 10^{\left(-\frac{RL_b}{10}\right)} \Bigg\} \cdot 10^{\left(-\frac{IL_{CIRi}+IL_{PSC2i}}{10}\right)} \end{aligned} \tag{2}$$

where $P_{in(i)}$ is the input power, $T_i(x)$ is the fiber transmission coefficient associated with fiber attenuation coefficient α_i[dB/km], which can be written as: $T_i(x) = \exp(-\alpha_i x)$. DIR [dB] is the directivity of the CIR (i.e., power transmitted directly from port 1 to port 3). IL_{WS}, IL_{OS2}, IL_{CIR} and IL_{PSC2} are the insertion loss (in dB) of the WS, OS_2, CIR, and 1×2 PSC_2, respectively. α_{C} is the connection loss between the channel #2 of the 1×2 OS_2 and the corresponding fault DF link. RL_{WS} and RL_{OS} represent the return loss (in dB) of the WS and OS. $RAY_i(x)$ is the Rayleigh backscattered power coefficient can be expressed as [20]

$$RAY_i(x) = \frac{1}{2\alpha_i} \cdot S_i \cdot \alpha_{Si} \cdot \left(1 - e^{-2\alpha_i x}\right) \tag{3}$$

α_{si} is the scattering coefficient due to the Rayleigh scattering and is inversely proportional to the fourth power of the wavelength. x is the length of the fiber segment and S_i is the capture coefficient. Since the proposed PON monitoring system uses two BLSs with different center wavelengths, and the parameters such as fiber transmission coefficient and Rayleigh backscattered power coefficient are wavelength dependent, we add subscript i ($i = 1$ for λ_{M1} and $i = 2$ for λ_{M2}) to indicate the values at different wavelengths. Note that insertion loss is wavelength sensitive while return loss is not [20].

In Eq. (2), except for x_b and RL_b, all other parameters are fixed and known, and two total received power (i.e., P_{TB1} and P_{TB2}) can be obtained by an optical power meter. Obviously, two $P_{in(i)}$s generated by different BLSs can construct two equations. Then, two unknown variables (i.e., x_b and RL_b) in Eq. (2) can be solved. When the fiber attenuation coefficient in the fiber under test corresponding to center wavelengths of the two BLSs used satisfy a certain relationship, for instance, $\alpha_1 = \alpha_2$ or $2\alpha_1 = \alpha_2$, the two variables in Eq. (2) can be analytically solved. For other cases, a numerical solution with good accuracy can be obtained by the least square method. In theory, the analytical solution may have higher localization accuracy. For the most widely used G.652D fiber, the fiber attenuation coefficient at 1310 nm and 1650 nm is approximately 0.34 dB/km and 0.3 dB/km. Therefore, we can easily find a center wavelength with a fiber attenuation coefficient of 0.3 dB/km between 1310 nm and 1550 nm.

The multiple-customers interference probability (MCIP), an important system performance, has been first proposed in [15], and it is closely related to the length difference of each DF link. As a two-dimensional coding scheme, the optical frequency hopping/periodic coding (OFH/PC) scheme in [15] has advantages in network monitoring capacity and MCIP compared with the classical periodic coding (PC) scheme [17]. Specifically, we use the Monte Carlo method to calculate the MCIP of 64 end-uses randomly distributed in a circular area with a radius of 50m at 10^5 times iteration. In this calculation, the pulse duration of the detection signals used in both the PC and OFH/PC schemes are 1 ns, and the code weight in the PC scheme is set to 4. All codes used in the OFH/PC scheme are selected from the code set (7, 2, 4, $P_i = 4, 7, 11$). The MCIPs of OFH/PC scheme does not exceed 0.004 while that of the PC scheme is roughly 0.7308. Due to the identification in the frequency domain, the proposed PON monitoring system is better than these two schemes in term of MCIP performance.

III. Experimental Demonstration

To illustrate the feasibility of the proposed PON monitoring system clearly, we divide the experimental demonstration into two parts: fault detection and fault localization. Limited by the existing facilities in the laboratory, we exploit bands commonly used in fiber optic communications instead of U-band as recommended by ITU-T for the proof-of-concept experiment. That is, the center wavelengths of the two SLDs used are 1310 nm and 1550 nm, respectively. Firstly, in a simplified 1×4 PON system, we intentionally introduce a break on a DF link to simulate the fault detection process. Note that the fault detection of each DF link is based on the spectra recognition. Secondly, we use the established equation to calculate the location of the breakpoint on the corresponding fault DF link. The calculated results of fault localization method are also compared with the OTDR measurement results.

A. Fault Detection

The detection signal emitted from the SLD_1 with center wavelength of 1550 nm and then sent to the network using a CIR;

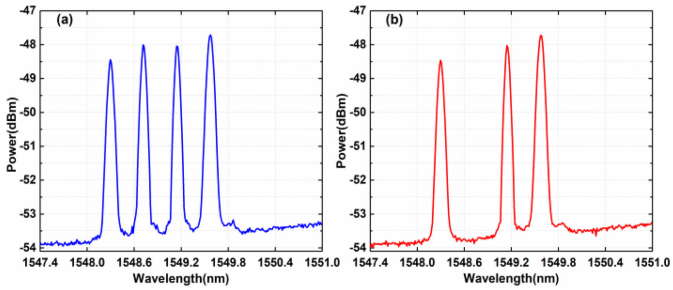

Fig. 3. Experimental results of fault detection: (a) All DF links are normal. (b) The DF_2 link occurs a break.

a 20.363 km fiber plays the role of FF, and a 1 × 2 mechanical OS and 1 × 4 PSC jointly serve as the RN. The 1 × 2 OS (i.e., OS_2) is placed on channel #1 and connected to the 1 × 4 PSC and FF. The distance difference between each DF link is less than 20 m, corresponding to a dense PON. Specifically, the DF_2 link and DF_3 link are equal in length. The FF and four DFs used are the same fiber type and from the same manufacturer. The 3-dB bandwidth of the FBGs used at the end of four DF links are roughly 0.1 nm. The CRWs of the FBGs corresponding to four DF links are 1548.29 nm, 1548.71 nm, 1549.14 nm and 1549.57 nm, respectively. The CRWs used are concentrated in a small range to better simulate the situation of more end-users in the full spectrum width. An optical spectrum analyzer (Anritsu MS9740A) with resolution of 0.03 nm is employed for the spectra recognition. The experimental results of fault detection are shown in Fig. 3. Fig. 3(a) shows that all four DF links are in a normal state. The corresponding reflection peak is absent as a break occurs on the DF_2 link, which is shown in Fig. 3(b). The absence of the corresponding reflection peak indicates that the faulty DF link is successfully detected. Fiber bending and connector misalignment are probably the most common difficulties in PON systems, particularly on the ONU side. However, these two types of failures cannot be distinguished by existing fault detection schemes. Recall that most existing fault detection schemes and the proposed fault detection technology mainly focus on fiber break. In the experiment of the fault detection part, we only simulate the case of fiber break. Multiple fiber break simulations on the same DF link show the absence of corresponding reflection peaks.

B. Fault Localization

In the experiment, three fiber breakpoints are introduced sequentially on the 4 km long DF_2 link. The 1 × 2 OS_1 switches to the channel #2 and connect the corresponding fault DF link. The BLS_1 (i.e., SLD_1) is operated at 1550 nm, which is the same as the transmitter module in the fault detection experiment. The two-input power (P_{in}) at 1550 nm and 1310 nm output from the transmitter module to the port 1 of the CIR are 7.41 mW and 6.09 mW, respectively. Note that two detection signals are injected into the network sequentially through the 1 × 2 OS_1 switching. The total backscattered and reflected power received (i.e., P_{TB1} and P_{TB2}) twice is directly measured by an optical power meter. The connection between the various devices adopts fiber fusion splicing to reduce the connection loss and unnecessary reflection. The main parameters used in the established equation are listed in Table I. The insertion loss of the CIR and 1 × 2 OS_2 at 1550 nm and 1310 nm are 2.21 dB and 2.02 dB, 0.8 dB and 0.68 dB, respectively. $S{\cdot}\alpha_s$ can be calculated by connecting an optical isolator to the end of the FF with known length.

TABLE I
THE MAIN PARAMETERS USED IN THE ESTABLISHED EQUATION

Detection central wavelength(*nm*)	L_{FF} (km)	$S{\cdot}\alpha_s$ (dB/km)	α (dB/km)	DIR (dB)	RL_{OS2} (dB)
1550	20.363	0.00022	0.19	60	55
1310	20.363	0.00048	0.33	60	55

TABLE II
COMPARISON BETWEEN OTDR MEASURED RESULTS AND THE CALCULATED RESULTS

Calculated result	OTDR measured result
3007m	3012m
1997m	2005m
999m	1004m

To verify the feasibility of the proposed fault localization method, three breakpoint locations has also been measured by a commercial OTDR. It can be clearly seen from Table II that the fault localization method has a small error with the OTDR measured results.

In the above measurement, the OTDR requires 2∼3 minutes for the averaging process. In contrast, the proposed fault localization method only takes several seconds. Based on the same transmitter module shared with the fault detection technology, the proposed fault localization can locate the breakpoints without OTDR intervention. From a cost point of view, the proposed fault localization method is cost-effective compared with the use of OTDR.

IV. ANALYSIS AND RESULT

A. Dynamic Range of Fault Detection

For the convenience of final spectra recognition, the reflection spectra of all FBGs used should not overlap each other in the frequency domain. Assuming that all FBGs have the same reflection bandwidth and different CRWs. The reflection bandwidth for a FBG is that between the first zeros on either side of the maximum reflectivity (i.e., peak reflection wavelength). Theoretically, smaller interval between the CRWs of different FBGs is conducive to efficient bandwidth usage of the BLS. Considering that the spectral width of the BLS is 40 nm and the reflection bandwidth of the FBG is 0.2 nm, the proposed system can monitor a PON with 64 end-users when the wavelength interval is 0.634 nm.

The wide spectral width of the BLS brings huge potential for network monitoring capacity, however, the extremely wide spectrum may also cause uneven power distribution in the entire spectrum. Here, we can comprehensively consider the spectral flatness (denoted as ΔF) and the DF link length to further

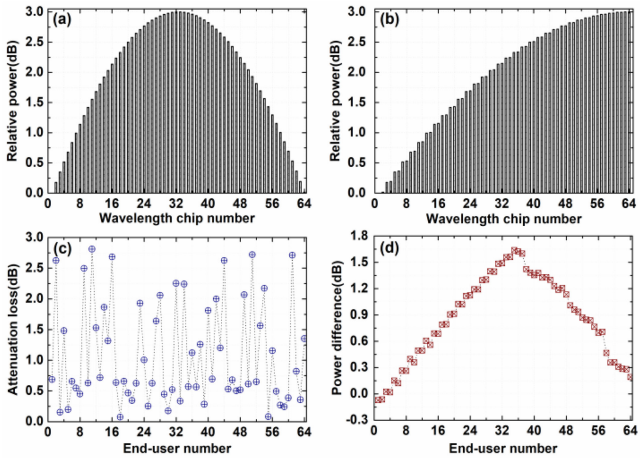

Fig. 4. Dynamic range calculation:(a) original wavelength chip;(b) allocated wavelength chip;(c) attenuation loss of each DF link;(d) power difference of the return signals.

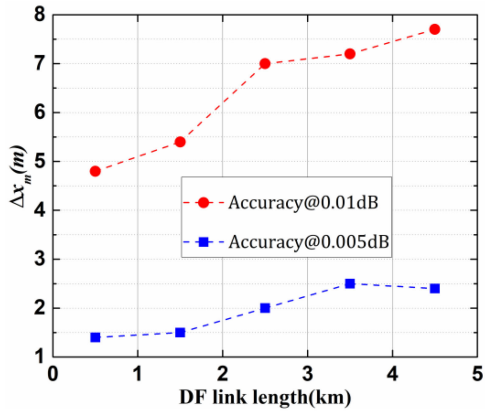

Fig. 5. The possible measurement error versus different accuracies.

reduce the requirements for the dynamic range of the recognition device. The output spectrum of the BLS approaches a Gaussian profile and it can be expressed as: $L(\lambda) = exp\ [-(\lambda-\lambda_c)^2/2\sigma_S^2]$, where λ_c and σ_S are respectively the central wavelength and the spectral width of the BLS [21]. Available wavelength chips can be calculated with $\lambda_c = 1650$ nm, $\sigma_S = 40$ nm and $\Delta F \leq 3$ dB, as illustrated in Fig. 4(a). In this calculation, the wavelength chip with the minimum power is set as the reference zero point. These wavelength chips are arranged in ascending order of power to facilitate the allocation, as shown in Fig. 4(b). When the power of each wavelength chip is fixed, the dynamic range is determined by the geographical distribution of end-users. Here, we also use Monte Carlo simulation with 10^5 times iteration to simulate the random distribution of various end-users' geographic locations. The maximum separation length in the PON with 64 end-users is less than 5 km. A 0.3 dB/km fiber loss is considered for U-band detection signal. Note that each iteration would produce a geographical distribution situation. For the sake of generality, we choose the situation with the highest dynamic range requirement as the final dynamic range. The geographical distribution of 64 end-users corresponding to the final dynamic range is shown in Fig. 4(c). After the wavelength chip is allocated to the corresponding DF link, the power difference of each return signal can be maintained in a small range, as shown in Fig. 4(d). In general, the high-power wavelength chip is allocated to long DF link while the low-power wavelength chip is for the short one. Obviously, these power differences indicate that the dynamic range does not exceed 1.71 dB. That is, the spectral flatness of the BLS can be used to reduce the dynamic range requirements of the spectra recognition device. Furthermore, the reflectivity of each FBG can also be used to flexibly adjust the dynamic range requirements.

B. Measurement Error of Fault Localization

Assuming that the minimum measurable power of the optical power meter is -70 dBm, we investigate the possible maximum measurement error (denoted as Δx_m) of the DF link length every 1 km within the range of 5 km. Recall that x_b and RL_b are a set of solutions in the binary linear equations constructed by Eq. (2). Note that the typical parameter specification of return loss ranges from 15 to 60 dB. The reflectivity of the fiber end is usually not more than 1% in most cases [22]. Consequently, the RL_b value corresponding to x_b in the same set of solutions is limited to between 20 dB and 60 dB. Fig. 5 shows the possible maximum measurement errors at different accuracies (i.e., 0.01 dB and 0.005 dB) when the length of the DF link is within 5 km. Note that the points at different accuracies are not a specific length, but the comprehensive calculation results within a given length range. For instance, the point of 4.5 km in Fig. 5 is actually the maximum difference of all possible measurable points for the DF link lengths in the range of 4 ∼5 km. Except for the range of 4 ∼5 km at the accuracy of 0.005 dB, the maximum measurement errors generally increase with the increase of the DF link length range at different accuracies. Within the same length range, the number of measurable points and the uniformity of the distribution of these points may determine the maximum measurable error. Compared with the range of 3∼4 km, the distribution of all measurable points within the range of 4∼5 km is relatively uniform, resulting in a smaller maximum measurement error. In this calculation, all measurable length solutions and their corresponding return losses are back-substituted into Eq. (2) to verify the accuracy of the solutions. When the length of the DF link is within 1 km, the Δx_m corresponding to the measurement accuracy of 0.01 dB and 0.005 dB are about 4.8 m and 1.4 m. As the length of the DF link increases, Δx_m generally shows an increasing trend under the two-measurement accuracy. When the length of the DF link is between 4 and 5 km, the Δx_m increases to about 7.7 m and 2.4 m respectively under the accuracy of 0.01 dB and 0.005 dB. Obviously, an optical power meter with higher measurement accuracy may greatly reduce the measurement error.

V. Conclusion

We have proposed and experimentally demonstrated an integrated PON monitoring system that can simultaneously complete fault detection and fault localization. The reflection spectra of FBGs with different CRWs used in fault detection can support

a large-capacity PON. With the same transmitter module in fault detection, the breakpoint can be successfully located using the established equation with two different BLSs. The maximum power difference between each return signal is not more than 1.71 dB, which can reduce the dynamic range requirements of the spectral recognition device. An optical power meter with a measurement accuracy of 0.005 dB, compared with a measurement accuracy of 0.01 dB, can reduce the possible maximum measurement error. The proposed system provides a simple and low-cost system construction that makes it a competitive practical solution in PON monitoring applications.

REFERENCES

[1] T. Horvath et al., "Passive optical networks progress: A tutorial," *Electronics*, vol. 9, no. 7, Jul. 2020, Art. no. 1081.

[2] J. A. Hernandez, R. Sanchez, I. Martin, and D. Larrabeiti, "Meeting the traffic requirements of residential users in the next decade with current FTTH standards: How much? How long?," *IEEE Commun. Mag.*, vol. 57, no. 6, pp. 120–125, Jan. 2019.

[3] T. Pfeiffer, P. Dom, S. Bidkar, F. Fredricx, K. Christodoulopoulos, and R. Bonk, "PON going beyond FTTH," *J. Opt. Commun. Netw.*, vol. 14, no. 1, pp. A31–A40, Jan. 2022.

[4] C. DeSanti, L. Du, J. Guarin, J. Bone, and C. F. Lam, "Super-PON: An evolution for access networks," *J. Opt. Commun. Netw.*, vol. 12, no. 10, pp. D66–D77, Oct. 2020.

[5] D. Z. Zhang, D. K. Liu, X. Wu, and D. Nesset, "Progress of ITU-T higher speed passive optical network (50G-PON) standardization," *J. Opt. Commun. Netw.*, vol. 12, no. 10, pp. D99–D108, Oct. 2020.

[6] R. Singh and M. Kumar, "A comprehensive analysis for the performance of next generation passive optical network," in *Proc. Int. Conf. Smart Gener. Comput., Commun. Netw.*, 2021, pp. 1–6.

[7] Calix, *Next-Generation PON: Eliminating physical Constraints from the Access Network*. San Jose, CA, USA: Calix, 2020.

[8] J. Zhang, M. Xu, H. Zhang, Z. Jia, and L. A. Campos, "Next-generation high-speed access network for emerging services," in *Proc. Conf. Lasers Electro-Opt. Pacific Rim*, 2020, pp. 1–2.

[9] M. A. Esmail and H. Fathallah, "Physical layer monitoring techniques for TDM-passive optical networks: A survey," *IEEE Commun. Surv. Tut.*, vol. 15, no. 2, pp. 943–958, Apr.–Jun. 2013.

[10] A. Usman et al., "Optical link monitoring in fibre-to-the-x passive optical network (FTTx PON): A comprehensive survey," *Opt. Switching Netw.*, vol. 39, Nov. 2020, Art. no. 100596.

[11] A. F. A. Asha'ari, A. A. A. Bakar, and N. F. Naim, "Design of optical frequency domain reflectometer (OFDR) interferometer based on fiber Bragg grating (FBG) for passive optical network (PON) monitoring," in *Proc. IEEE 7th Int. Conf. Photon.*, 2018, pp. 1–3.

[12] X. Zhou, F. Zhang, M. Sun, C. Pan, and X. Sun, "A modified optical coding monitoring scheme in PON with electronic decoding processing," *IEEE Commun. Lett.*, vol. 17, no. 9, pp. 1849–1851, Sep. 2013.

[13] X. Zhang et al., "Self-match based on polling scheme for passive optical network monitoring," *Opt. Commun.*, vol. 417, no. 15, pp. 19–23, Jun. 2018.

[14] M. P. Fernández, L. A. Bulus Rossini, and P. A. Costanzo Caso, "PON monitoring technique using single-FBG encoders and wavelength-to-time mapping," *IEEE Photon. Technol. Lett.*, vol. 31, no. 21, pp. 1745–1748, Nov. 2019.

[15] X. Zhou, F. D. Zhang, and X. Sun, "Centralized PON monitoring scheme based on optical coding," *IEEE Photon. Technol. Lett.*, vol. 25, no. 9, pp. 795–797, May 2013.

[16] M. P. Fernández, P. A. Costanzo Caso, and L. A. Bulus Rossini, "False detections in an optical coding-based PON monitoring scheme," *IEEE Photon. Technol. Lett.*, vol. 29, no. 10, pp. 802–805, May 2017.

[17] M. M. Rad, H. Fathallah, S. LaRochelle, and L. A. Rusch, "Experimental validation of periodic codes for PON monitoring," in *Proc. IEEE Glob. Telecommun. Conf.*, 2009, pp. 1–7.

[18] X. Zhang et al., "Fault localization using dual pulse widths for PON monitoring system," *Opt. Laser Technol.*, vol. 106, pp. 113–118, Oct. 2018.

[19] C. Gao and G. Farrell, "Equationling of Rayleigh backscattering in plastic optical fiber," in *Proc. High Freq. Postgraduate Student Colloq.*, 2003, pp. 14–17.

[20] M. Cen, J. Chen, V. Moeyaert, P. Mégret, and M. Wuilpart, "Advanced fault-monitoring scheme for ring-based long-reach optical access networks," *J. Lightw. Technol.*, vol. 35, no. 10, pp. 1876–1886, May. 2017.

[21] J. F. Huang, C. M. Tsai, and Y.-L. Lo, "Compensating fiber gratings for source flatness to reduce multiple-access interferences in optical CDMA network coder/decoders," *J. Lightw. Technol.*, vol. 22, no. 3, pp. 739–745, Mar. 2004.

[22] Z. H. Luo et al., "Fiber-end antireflection method for ultra-weak fiber Bragg grating sensing systems," *Meas. Sci. Technol.*, vol. 32, no. 5, Mar. 2021, Art. no. 055109.